

CPIA PUBLICATION 457  
VOLUME I  
OCTOBER 1986

Reproduction not authorized except  
by specific permission from CPIA.

# 23rd JANNAF COMBUSTION MEETING

VOLUME I



NASA-LANGLEY RESEARCH CENTER

Hampton, Virginia

20-24 OCTOBER 1986

**CHEMICAL PROPULSION INFORMATION AGENCY**

Operating under contract N00024-85-C-5301

THE JOHNS HOPKINS UNIVERSITY • APPLIED PHYSICS LABORATORY • LAUREL, MD.

Approved for public release; distribution is unlimited.

MEASUREMENTS OF PARTICULATES  
IN SOLID PROPELLANT ROCKET MOTORS

T. Edwards, K.G. Horton, D. Redman, J.S. Rosa,  
J.B. Rubin, S.C. Yoon, J.P. Powers, D.W. Netzer

NAVAL POSTGRADUATE SCHOOL  
MONTEREY, CALIFORNIA 93943-5100

ABSTRACT

An investigation has been conducted to develop techniques for obtaining quantitative data that can be used to relate solid rocket propellant composition and operating environment to the behavior of solid particulates within the grain port and exhaust nozzle. The techniques employed are high speed motion pictures of propellant strand burners and slab burners in a cross-flow environment, SEM analysis of post-fire residue (strand, slab, and motor), determination of  $D_{32}$  across the exhaust nozzle using measurements of scattered laser light, and holograms of burning propellant strands, slabs, and motors. In addition, techniques are being developed for automatic retrieval of particle size distributions from holograms taken of the combustion of solid propellants. Results are presented on (1) the measurement of particle size changes across an exhaust nozzle, (2) holograms obtained at the grain exit plane and (3) progress on the automatic retrieval of particle data from the holograms.

INTRODUCTION

Aluminum is added to solid propellants to increase performance and to suppress high-frequency combustion instabilities. A small amount of a variety of additives in addition to aluminum (aluminum oxide, zirconium, etc.) are also used in reduced-smoke propellants for acoustic stabilization. In addition, there is renewed interest in dense additives ( $\text{Bi}_2\text{O}_3$ , etc.) in order to provide higher performance with low hazards propellants. Although the delivered specific impulse of metallized propellants is higher than that of the base propellants, the specific impulse efficiency is lower. This results from the presence of condensed metal oxides in the nozzle flow and from unburned metal within the motor port. Some particles, upon reaching the burning surface, depart immediately while others agglomerate on the surface before passing into the gas flow. Most of the metal combustion is thought to occur in the gas phase, resulting in small (typically less than two microns) metallic oxide particles. These particles are of major significance in determining the exhaust signature. In addition, particle burnout can also result in the break-up of a metallic oxide cap or layer. This can result in larger (greater than five microns) particles. The larger particles are more important in the determination of two-phase flow losses in the exhaust nozzle flow since they can lag the gas flow and, in principle, could be affected through propellant changes. There are several rather complex computer codes [Ref. 1] which attempt to model the important processes of momentum and thermal energy exchange between the solid, liquid, and gaseous phases as well as particle collisions, break-up, and wall collisions. However, these models remain semi-empirical and are generally based upon particle size distributions which were obtained from collected nozzle exhaust flows [Ref. 2]. Particle histories from the surface of the propellant to the nozzle exit remain largely unknown, due to the difficulty of making direct measurements within the motor and nozzle. Prediction of performance losses due to the presence of the original metal and the metal oxides are very sensitive to the assumed particle size distribution, and essentially no data are available that give this distribution as a function of position throughout the motor and nozzle.

Collecting exhaust products is feasible only for small rocket motors. Even then, the techniques employed result in considerable variation in the measured sizes [Ref. 2]. Dobbins [Ref. 3] and Dobbins and Strand [Ref. 4] attempted to use an optical technique for measuring exhaust particle size and to compare the measurements with tank collected exhaust results. The optical technique used was a three-wave-length transmission measurement. This technique requires knowledge of particle index of refraction and the standard deviation of the particle size distribution. The optical measurements generally yielded sizes which were too small and the results were inconsistent with the collected exhaust data. It was speculated that this discrepancy resulted from a bi-modal exhaust particle distribution.

This work was performed under Contract Number F04611-86-X-0008 with the Air Force Rocket Propulsion Laboratory, Edwards, California.

Approved for public release; distribution is unlimited.

Light transmission measurements have the advantage of being applicable to dense concentrations where multiple scattering occurs [Ref. 5]. However, the method works best for small particles (on the order of the wavelength of the illumination source) and requires a-priori knowledge of the particle characteristics.

Light scattering measurements can also be used to determine particle size [Refs. 6-15]. If the scattering angles used are specifically selected, the technique can be used to look almost entirely at one lobe of a bi-modal size distribution. Ratioing intensities obtained at two forward scattering angles can be used to further reduce the complexity of the method. However, scattering techniques are generally thought to be applicable only to systems where the transmittance is greater than approximately 90% in order to satisfy single scattering requirements.

A combination of light transmission and light scattering measurements [Ref. 13] appears to be well-suited for many solid propellant rocket motor exhaust flows. However, experimental efforts are first needed to determine under what conditions (metal loadings, operating pressure, propellant ingredients, etc.) light scattering measurements can be made in this difficult environment.

The goal of the investigation to date has been to develop and compare experimental techniques that can be used for obtaining quantitative data on the effects of propellant properties, operating pressure, and nozzle geometry on the behaviour of metallized particulates within the grain port and nozzle of solid propellant rocket motors. These data are needed in order to (1) improve solid propellant performance predictive capabilities, (2) provide needed input to current steady-state combustion models which include oxidizer-metal interactions, (3) provide data on the effects of motor and propellant conditions on exhaust signature and (4) provide in-motor particle size distributions which will allow more accurate predictions of damping in stability analyses. The techniques employed have been high speed motion pictures of strand burners and slab burners in a cross-flow environment, SEM analysis of post-fire residue (strand, slab, and motor), determination of changes in  $D_{32}$  across the exhaust nozzle using measurements of scattered laser light, and holograms of burning propellant in strands, slabs, and motors. In addition, considerable effort has been directed toward development of automatic data retrieval methods for obtaining particle size distributions from holograms taken of the combustion of solid propellants. The holographic effort is a two-part problem. Techniques must be developed for obtaining good quality holograms in a realistic solid propellant combustion environment. However, these holograms are of limited value unless the particle size data can be obtained from them in a reasonable time period. This requires development of computer-aided image analysis techniques.

Previous results from this continuing investigation are presented in References 16-18. This paper summarizes some of the earlier results and presents recent results obtained using both measurements of diffractively scattered light and holography in a small solid propellant rocket motor.

## DETERMINATION OF PARTICULATE SIZE USING MEASUREMENTS OF SCATTERED LIGHT

### INTRODUCTION

The method used in the present effort is the diffractively scattered light technique. The diffraction patterns of light scattered by particles are analyzed to determine the volume-to-surface mean diameter ( $D_{32}$ ). This method has the disadvantages that size distributions cannot be easily determined and particles larger than some threshold size will not be detected due to the exceedingly small angles at which they scatter light. However, it has the advantage that it is non-intrusive and, in theory, can be used in the internal motor environment. Propellant composition can limit the application of the technique by producing large particulates and/or very dense particle clouds.

The completely general theory of scattering was developed by Mie and is presented by Van de Hulst [Ref.15]. The light scattering characteristics for spherical particles of any size are fully described and the phenomena of reflection, refraction, diffraction and extinction are considered. For particle sizes much smaller than the wavelength of the illuminating light source, the Mie equations simplify to what is called Rayleigh scattering.

The size of the particles of interest in solid propellant rocket motor combustion depends upon the application. Most applications are concerned with particles having diameters much greater than the wavelength of visible light. Scattering by these larger particles is described by Fraunhofer diffraction. Measuring the particle size for a monodispersion can be accomplished by measuring the angular position of a dark or bright ring in the diffraction pattern. This method is not used for polydispersions since the discrete rings are not observed. However, Dobbins, et al [Ref.7] found that the volume-to-surface mean diameter of a polydispersion ( $D_{32}$ ) defined by

$$D_{32} = \frac{\int_0^{D_{\max}} N_r(D) D^3 dD}{\int_0^{D_{\max}} N_r(D) D^2 dD} \quad (1)$$

(where  $N_r(D)$  is a distribution function describing the proportion of particles with diameter  $D$  in the sample), could be accurately measured. The value of  $D_{32}$  was shown to be quite insensitive to the form of  $N_r(D)$ . In addition, since the ratio of forward scattered light at two angles is dominated by Fraunhofer diffraction, it is insensitive to the particle refractive index and the particle concentration [Ref.13]. To evaluate the integrated intensity over all particle sizes requires specification of  $N_r(D)$ . Dobbins, et al [Ref.7] used the Upper-Limit-Distribution-Function developed by Mugele and Evans [Ref.9] and this approach was followed in the present investigation.

For  $\pi D_{32} \theta / \lambda$  (where  $\theta$  is the scattering angle and  $\lambda$  is the wavelength) less than 3.0, a Gaussian curve [Ref.14] can be used which closely matches the theoretical intensity profile obtained by integrating the Fraunhofer diffraction expression together with the Upper-Limit-Distribution-Function [Ref.7]. This Gaussian expression has been presented by Buchele [Ref.14] and is given by

$$I_{\theta} / I_{\theta=0} = \exp - (0.57\pi D_{32} \theta / \lambda)^2 \quad (2)$$

Equation (2) can be used to obtain the intensity ratio between two (within the apparatus limits) forward scattering angles:

$$I_2 / I_1 = \exp - D_{32}^2 [(\theta_2^2 - \theta_1^2) (0.57\pi / \lambda)^2] \quad (3)$$

#### EXPERIMENTAL APPARATUS AND PROCEDURES

Figure 1 is a schematic of the apparatus and Figure 2 is a schematic of the small motor which was used. The light scattering equipment was mounted on two optical benches; one for measurements in the nozzle exhaust and one for measurements within the motor cavity. The light sources employed were eight milliwatt helium neon lasers.

Each beam passed through the appropriate test volume and was then intercepted by a physical stop located in front of the receiving optics. The further the stop was placed from the test section, the smaller was the angle at which scattered light could be measured. The upper limit of the scattering angle is determined by the diameter and focal length of the focusing lens, the distance between the focusing lens and the particles, the diameter of the motor window, or the height/position of the diode array. In the present apparatus scattered light could be measured within an angle increment of approximately 0.05 radians. The minimum possible scattering angle was approximately 0.008 radians and the maximum approximately 0.07. These angles can be changed by changing one of the above limits. The presently employed angle limits introduce some bias in the collected data.

The scattered light passed through a laser line filter and a 50cm focal length lens which focused the light onto the linear diode array. The arrays each contained 1024 silicon photodiodes on a single chip with 25 micron spacing. The accompanying circuits provided a "sampled and held" output which was essentially analog except for switching transients. The actual sampling time of the array was about 34 msec with a delay between scans of about 6 msec. Currently the system is being improved to permit sampling in approximately 4 msec.

Raw data was plotted on the CRT where any obviously erroneous scans could be excluded from further data reduction. The valid scans were averaged to obtain a mean scattering profile. The mean intensity profile taken before particles were introduced was then subtracted from that taken with particles present. This corrected for the characteristics of individual photodiodes and extraneous light which was independent of the particles.

A symmetric moving-average-type of digital filter was then applied to the profile to achieve smoothing. This type of digital filter was chosen for simplicity and because it does not have the phase lag of analog filters. Smoothing of the data has been found to be necessary if good results are to be obtained using the two-angle methods when only a few scans of the array are possible (as in time-dependent combustion).

Calibration of the apparatus was accomplished by measuring  $D_{32}$  of various particles of known size distribution. Polydispersions of glass or polystyrene spheres and aluminum oxide powder were suspended in water within a Plexiglas or glass container. A scanning electron microscope (SEM) was also used to photograph each particle sample.

Figure 3 illustrates that the present system can be used to measure particles with an accuracy of approximately  $\pm 0.5$  microns. Table I shows that the scattering measurements can provide good particle size data well into the multiple-scattering regime. Table II presents some of the calibration results.

TABLE I TRANSMITTANCE EFFECTS ON SCATTERING MEASUREMENTS

TRANSMITTANCE, %	D <sub>32</sub> , MICRONS
85	10
70	10
60	9.5
50	9.5
30	9

TABLE II CALIBRATION RESULTS FOR LIGHT SCATTERING APPARATUS

PARTICLE MATERIAL	SAMPLE PARTICLE SIZE RANGE (microns)	CALCULATED D <sub>32</sub> (microns)	MEASURED D <sub>32</sub> (microns)
Polystyrene	3-6	4.7**	4.5
Polystyrene	6-16	10.2**	10.0
Polystyrene	15-30	21.6**	21
Glass	37-44	38*	40
Glass	53-63	54*	54-58
Glass	1-37	25*	28-30

\* From SEM photographs      \*\* From Manufacturers Data

The results of the calibration tests showed that the apparatus is capable of accurately measuring mean particle size for a broad range of mean diameters providing that size range is not too wide.

#### MOTOR FIRING RESULTS

Table III summarizes the conditions employed for the first tests.

TABLE III CONDITIONS EMPLOYED FOR INITIAL MOTOR FIRINGS

Burn Time	= 2.5 sec
P <sub>c</sub>	= 300-500 psia
Residence Time	= 12 msec
Propellant	: 14.7% GAP
	45.7% 200 micron, 24.6% 25 micron AP
	8.5% TEGIN
	4.8%, 2%, or 0%, 20 micron Al (same solids loading)

Light scattering measurements were made in the exhaust jet of the converging nozzle. The non-metallized propellant tests were made to insure that the temperature/density gradients were not effecting the sizing measurements. Particles were also collected from the motor wall at the nozzle entrance (adjacent to the viewing windows) and from the walls of the exhaust collection tube. Results are presented in Table IV. Although the collected samples were quite small (and perhaps biased), these results indicated that the measurement technique appeared to be reasonably accurate. It should also be noted that the particle size appeared to be time-dependent since each test was made at different positions along the pressure-time trace.

TABLE IV RESULTS FROM INITIAL MOTOR FIRINGS

<u>Weight % Al</u>	<u>Measured D<sub>32</sub> in Exhaust (microns)</u>	<u>SEM D<sub>32</sub> (Motor/Exhaust) (microns)</u>
4.8	5.6	10.2/5.6
4.8	5.5	—
4.8	12.0	18.9/13.6
2.0	7.0	14.4/12.2
2.0	9.3	—
2.0	4.6	10.8/4.9

The particle size distribution which leaves the propellant surface, and subsequently changes due to combustion, is a complicated function of the propellant composition and the motor operating conditions. To help separate the effects of the gas phase processes from the propellant surface processes the apparatus was modified. The motor was mounted vertically with a particle injection device attached at the head-end. Particles of known composition and size distribution could then be introduced into the motor. In these tests a non-metallized propellant (15% HTPB, 85% AP) was used to provide the hot gas environment and the particle mean sizes were again measured at the entrance and exit of the exhaust nozzle.

High speed motion pictures and holograms of the particles as they dropped through the motor in non-burning tests indicated that they were uniformly distributed within the motor aft of the propellant grain.

Initial tests were conducted using both 25 micron glass beads and 23 micron Al<sub>2</sub>O<sub>3</sub> at pressures between 200 and 300 psia. These large particles had only short residence times (~3 msec) within the propellant grain and residence times of approximately 50 msec to the motor windows. This, together with the particle compositions, resulted in very little particle change from injection to nozzle entrance. Interestingly, there was also very little change in particle mean diameter across the nozzle. The measurements of D<sub>32</sub> from light scattering were somewhat smaller than the D<sub>32</sub> obtained from the collected particles. Several problems were evident in these tests. The collected samples were biased from particles which continued to fall after motor burn-out and particle impingement on the propellant surface resulted in rapid increases in chamber pressure.

#### SUMMARY

The light scattering technique appears to work quite well, although apparatus improvements are required to improve the quality of the obtainable data. Currently the propellant port diameter is being enlarged to minimize the surface impingement problem and aluminum is being injected rather than glass or Al<sub>2</sub>O<sub>3</sub>. In addition, faster (500 KHZ) A/D converters and larger data memory units are being used. A Malvern 2600 HSD particle size analyzer has also been recently obtained and will be used to obtain particle size distributions to compare with results obtained with the present apparatus.

#### HOLOGRAPHIC INVESTIGATION

The holographic investigation uses a holocamera surrounding the small windowed rocket motor together with a one joule, pulsed (50 nsec) ruby laser. Hologram reconstruction is accomplished using a 0.5 watt cw Krypton laser. Viewing of the reconstructed hologram is done through a microscope. The observed images can be recorded on film (3 x 5 Polaroid or 35 mm) or on a videocamera for further processing.

Resolution limits have been determined using both the Air Force resolution (bar) target and the Laser Electro-Optics Calibration Reticule (particles). These calibration tests have been made using both diffuse and collimated scene beam illumination and both pulsed ruby and cw krypton lasers. The best resolution obtained to date is four microns, with eight microns being more typical.

Smoke (submicron particles) limits the metal loadings and operating pressures where holograms can be obtained. Laser transmittance tests are initially made through the motor to determine where holograms can be obtained (generally when  $T > 10\%$ ) and to determine the filtering required to obtain the desired scene beam to reference beam intensity ratio. In addition, diffuse scene beam illumination is generally required to smear the schlieren effects which result from the multitude of burning particles. To date, good quality holograms have been obtained to pressures of 280 psi using an HTPB/AP propellant with 2%, 20 micron aluminum.

#### AUTOMATED DATA RETRIEVAL FROM ROCKET MOTOR HOLOGRAMS

The goal of this portion of the investigation is to automate the retrieval of statistical size information of the particles from the holograms recorded within the rocket motor. In order to do this, it is necessary to perform the following steps:

- record the hologram image on video tape,
- digitize the image on the computer,
- reduce the speckle of the image so that the particles may be identified as features of interest,
- separate the features from the background by removing the background,
- isolate and locate the features, and obtain a count of the total number of features within the field of view,
- obtain size information on area, x-width, y-width, and roundness, and
- produce a histogram of the particle size distribution.

Each of these steps will now be described in some detail.

#### IMAGE RECORDING

The image acquisition process is illustrated in Fig. 4. The holocamera is mounted on a precision x-y-z stage and illuminated with the reconstruction laser beam. A real image is formed in front of the hologram. It is sometimes useful to place a spinning mylar disk at the location of the image. If the disk spins faster than the integration time of the detector, then some speckle reduction occurs due to the averaging effect of the speckle background while the particle images remain in registration. The image is viewed through magnifying microscope objective. Values of 2X, 4X, and 10X are used. As the magnification increases, the field of view of the lens decreases, causing the total amount of light to decrease significantly at the higher magnification. A high-sensitivity (0.5 lux) television tube allowed the image to be successfully recorded on a VHS tape recorder at all magnifications.

#### IMAGE DIGITIZATION

The image digitization was done by feeding the tape image into a commercial image digitization board made by Imaging Technology, Inc. for the IBM PC/AT microcomputer. This board can digitize a 512x512 image into 256 gray levels ranging from 0 (black) to 255 (white). While pseudocolor output is available, the processed and raw images were displayed only in black and white. A companion set of software is available with the board. This software offers standard image processing capabilities including:

- image snap, grab and average modes for images presented over the standard RS-170 video input,
- output mapping functions that allow a wide variety of linear and nonlinear mapping of the input gray scale into an output gray scale,
- several standard image processing algorithms are available including, for example, the Laplace operation, convolution operations, and the Sobel operation,
- several manipulations of the image geometry such as image rotation, mirror inversion, and others, and
- graphic operations allowing one to annotate the image.

The software is available in two forms. The first is a closed, mouse-driven system that has proven useful for quickly evaluating various operations and finding the numerical values that can be used in the processing. The second form is a set of Pascal subroutines that can be imbedded in dedicated programs and that allow the user to transfer data into the computer for use in other programs such as statistical analysis and plotting operations. The routines are compatible with Microsoft versions of Fortran, C and Pascal compilers. Fortran was used in our investigations.

## SPECKLE REDUCTION

The separation of the features from the background is done with a thresholding operation. All pixels with a grey level below a certain value are called a feature pixel; all pixels above that grey level are considered background and will be set to value 255. This technique of producing a binary image assumes that the features and background will have separable ranges of grey scale; an assumption that is not true for the raw image.

The holograms are recorded with a diffuser present in the illumination path to avoid recording phase variations associated with the complicated thermal gradients in the rocket motor. The presence of this diffuser causes laser speckle in the background of the image. This speckle obscures the smaller particles and erodes the edges of the large particles as seen in the resolution target shown in Fig. 5a. In order to resolve the particles, it is necessary to reduce or remove the speckle. This speckle reduction effort has been the major thrust of recent efforts.

One method of reducing the speckle is to average several images with independent speckle patterns but with the particles in registration. This is the idea behind placing the spinning mylar disk in the image plane. The image processing board allows one to input several separate images and having the board perform the averaging computationally. This method showed that spinning the mylar disk in the image was equivalent to averaging about twenty separate images. No further improvement was discernable for the averaging technique beyond this. Since the spinning mylar was easier to implement than the computer averaging technique, subsequent images all used the mylar disk rather than the computational averaging.

Although the averaging technique lowers the speckle level, tests on applying the threshold show that significant misidentification of background as particles still occurs, calling for more reduction of the speckle level.

A speckle reduction technique was developed using a sequential application of a convolution filter, a threshold, and another convolution filter. The averaging of the convolution filters works to suppress the speckle. This technique was used to obtain the experimental results described below. It was found, however, that the accompanying reduction in resolution due to the smearing of the feature edges was too severe to be used for particles below twenty micrometer diameter, as is discussed in the section on experimental results below. Efforts were then begun on investigating speckle reduction filters that preserve the edges of objects within the image.

A survey of the literature showed that speckle reduction techniques have been of interest in the synthetic aperture radar field. Figure 5 shows a comparison of various speckle reduction methods that have been implemented. The speckle index is a statistically defined quantity [Ref. 19, 20] that allows a quantitative measure of the level of speckle in a region of the image. For our purposes, a 240x240 section in the upper left corner of the image proved to be representative of the overall speckle index of the image. Figure 5a shows the raw image. Figures 5b, 5c, and 5d show the results of implementing a geometric filter [Ref. 19], a "sigma" filter [Ref. 20] and a "statistical" filter [Ref. 20]. These filters are described in the literature referenced. All are judged to be relatively good at speckle reduction while retaining the edges of the features.

One of the major issues of reducing the speckle in an image is the resultant decrease in the resolution. An effort has begun to quantize this decrease in the resolution for each of the speckle reduction filters by using holograms of the USAF resolution chart recorded and reconstructed with our image acquisition process.

## FEATURE IDENTIFICATION

Once the threshold has been applied, and the particle features are extracted from the background, the next step in processing is the feature identification. To accomplish this an algorithm has been developed to locate connected pixels of the object. This algorithm looks for vertically and horizontally connected pixels. It currently does not find diagonally connected pixels. Processing steps are included to correctly identify features with holes in them ("doughnuts") and features that bend ("croissants"). All features are given a number from 1 to  $n$ , where  $n$  is the total number of features. The data array is then stored in the image memory location for the sizing operation.

## SIZING

In the sizing operation, an algorithm finds the maximum dimension in the horizontal and vertical dimensions. Special handling of objects with holes is required to correctly size these objects. Since the particles of interest are spherical, a test was included to eliminate non-round objects. It was found experimentally that any object whose x-dimension and y-dimension differed by more than two pixels were overlapping or clustered particles. Usually, only round objects were included in the data set.

## STATISTICAL ANALYSIS

A program was written to perform histogram analysis on the size data collected. This program was used to analyze the data presented below. Currently, evaluation of commercial statistical analysis packages available for the PC is being pursued.

## EXPERIMENTAL RESULTS

The system was used to analyse the data from a calibration object with known statistics. This object is a slide with circular depositions of known size and variation. The circles ranged from 5.33 to 92.78 micrometers in twenty-three nonuniform steps. A histogram of the manufacturer's data is shown in Fig. 6. This data was theoretically predicted for the measured response of a Malvern Particle Analyzer.

In comparing the manufacturer's data with the experimental results, we must remove the smaller diameter particles from the data sample since they are unresolved. All data to the left of the threshold at about 10 micrometers in Fig. 6 needs to be dropped. The exact location of the threshold is not known because of the stepwise nature of the particle diameter values used. (This is one of the reasons for the resolution study mentioned earlier.) Particles 8.85 micrometers and smaller cannot be resolved., while particles 11.56 micrometers and above are resolved. Each filter will have a different resolution threshold, causing the plots to look slightly different at the short wavelength end of the plots.

The first case presented is the calibration object when illuminated by white light, but subject to the same processing operations once stored in the computer. This case removed the limitations of the holography process and serves as a basis of comparison for the other cases studied. The resolution threshold for this case was between 11.56 and 17.47 micrometers. Figure 7a shows the truncated manufacturer's data, and Fig. 7b shows the experimentally measured data. (Note that the particle size is given in units of pixels rather than micrometers.)

The second case studied was a reconstruction of a diffuse hologram of the calibration object in the experimental setup (but with no motor firing). The resolution threshold for this case was between 21.38 and 23.91 micrometers. Figure 8a shows the truncated manufacturer's data, and Fig. 8b shows the experimentally measured data. (Again pixel units are used for the particle size.)

## SUMMARY

Since the resolution of the hologram case was not small enough to be useful (we require resolution of particles below 10 micrometers and ideally down to 1 micrometer), efforts were begun to study the resolution degradation phenomena to identify where the resolution was lost in an effort to improve the final result. These studies are continuing. Improved hologram geometries and film processing has led to better resolution in the reconstruction (currently about 5 micrometers). Analysis and comparison of the resolution degradation of the speckle reduction filters is in progress. Future work includes study of the effects of the grayscale threshold on the resolution of the processed image.

## REFERENCES

1. D. George, "Recent Advances in Solid Rocket Motor Performance Prediction Capability," AIAA Paper No. AIAA-81-033, 19th Aerospace Sciences Meeting, Jan 12-15, 1981.
2. R.W. Hermsen, "Aluminum Oxide Particle Size for Solid Rocket Motor Performance Prediction," AIAA 19th Aerospace Sciences Meeting, Jan 12-15, 1981.
3. R.A. Dobbins, "Remote Size Measurements of Particle Product of Heterogeneous Combustion," Eleventh Symposium (International) on Combustion, The Combustion Institute, 1967, p. 921.
4. R.A. Dobbins and L.D. Strand, "A Comparison of Two Methods of Measuring Particle Size of  $Al_2O_3$  Produced by a Small Rocket Motor," AIAA J. Vol. 8, 1970, pp. 1544-1550.
5. K.L. Cashdollar, C.K. Lee, and J.M. Singer, "Three Wavelength Light Transmission Technique to Measure Smoke Particle Size and Concentration," Applied Optics, Vol. 18, No. 11, June 1979, pp. 1763-1769.
6. R.O. Gumprecht and C.M. Slipevich, "Scattering of Light by Large Spherical Particles," J. Physical Chem., Vol. 57, Jan 1953, pp. 90-94.
7. R.A. Dobbins, L. Crocco, and I. Glassman, "Measurement of Mean Particle Size of Sprays from Diffractively Scattered Light," AIAA J. Vol. 1, No. 8, 1963, pp. 1882-1886.
8. J.H. Roberts and M.J. Webb, "Measurements of Droplet Size for Wide Range Particle Distributions," AIAA J., Vol. 2, No. 3, 1964, pp. 583-585.
9. R.A. Mugele and H.D. Evans, "Droplet Size Distribution in Sprays," Ind. and Eng. Chem., Vol. 43, 1951, pp. 1317-1324.
10. R.A. Dobbins and G.S. Jizmagian, "Optical Scattering Cross-Sections for Polydispersions of Dielectric Spheres," J. Optical Soc. of Am., Vol. 56, No. 10, 1966, pp. 1345-1350.
11. R.A. Dobbins and G.S. Jizmagian, "Particle Measurement Based on Use of Mean Scattering Cross-Sections," J. Optical Soc. of Am., Vol. 56, No. 10, 1966, pp. 1351-1354.
12. J.R. Hodgkinson, "Particle Sizing by Means of the Forward Scattering Lobe," Applied Optics, Vol. 5, 1966, pp. 839-844.
13. E.A. Powell, R.A. Cassanova, C.P. Bankston, and B. Zinn, "Combustion Generated Smoke Diagnostics by Means of Optical Measurement Techniques," AIAA Paper No. 76-67, AIAA 14th Aerospace Sciences Meeting, Jan 1976.
14. D.R. Buchele, "Particle Sizing by Measurement of Forward Scattered Light at Two Angles," NASA TP 2156, May 1983.
15. H.C. Van de Hulst, "Light Scattering by Small Particles," John Wiley and Sons, Inc., New York, 1957.
16. S.G. Karagounis, et. al., "An Investigation of Experimental Technique for Obtaining Particulate Behavior in Metallized Solid Propellant Combustion," Air Force Rocket Propulsion Laboratory Report, AFRPL-TR-82-051, July 1982.
17. R.G. Cramer, et.al., "An Investigation of Experimental Techniques for Obtaining Particulate Behavior in Metallized Solid Propellant Combustion," Air Force Rocket Propulsion Laboratory Report AFRPL-TR-84-014, Feb. 1984.
18. D.W. Netzer and J.P. Powers, "Experimental Techniques for Obtaining Particle Behaviour in Solid Propellant Combustion," AGARD-CP-391, No. 19, AGARD Conference on Smokeless Propellants, Florence, Italy, 12-13 Sept. 1985.
19. T.R. Crimmins, "Geometric Filter for Speckle Suppression," Optical Engineering, 24(10), pp. 1438-1443, 1985.
20. T.R. Crimmins, "Geometric Filter for Speckle Suppression," 24(4), pp. 651-654, 1986.
21. J.-S. Lee, "Speckle Suppression and Analysis for Synthetic Aperture Radar Images," Optical Engineering, 25 (4), pp. 636-643, 1986.

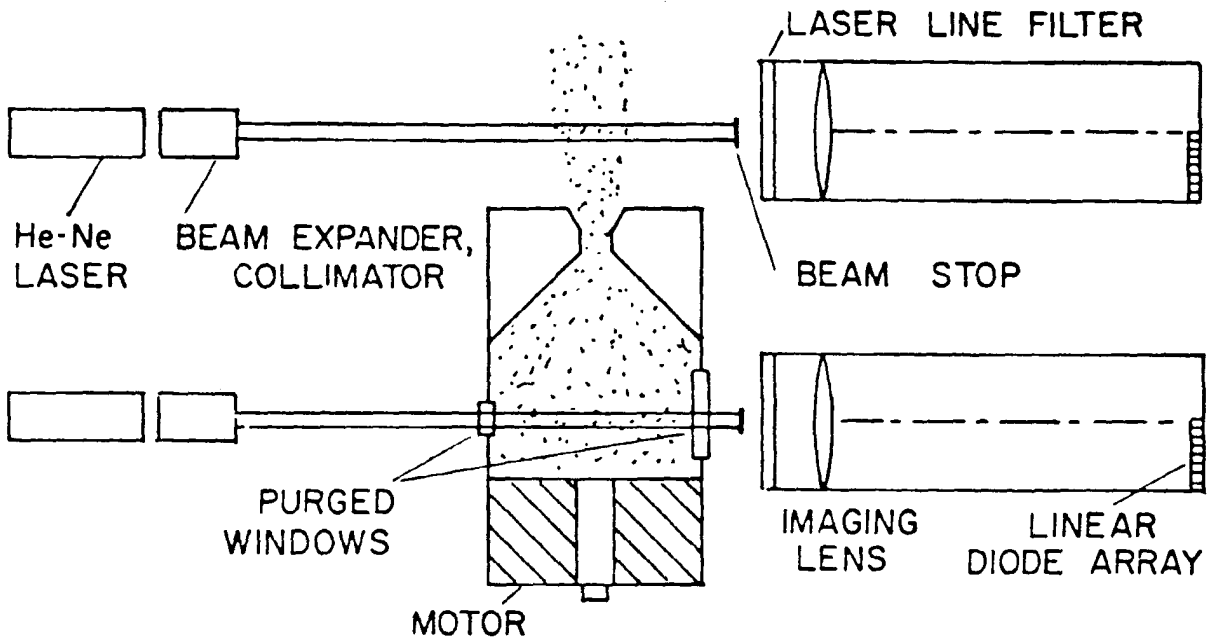


Figure 1. Schematic of Scattered Light Measurement Apparatus.

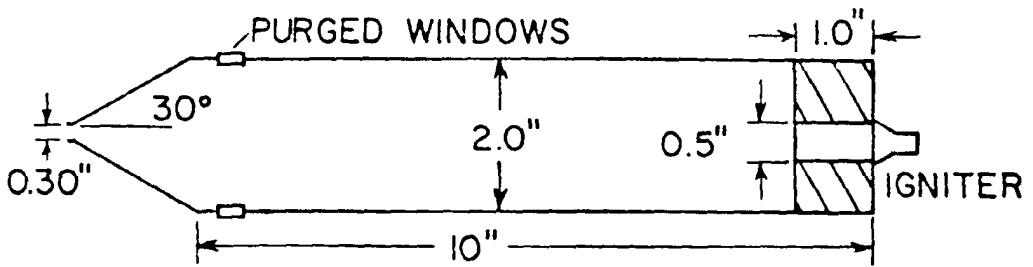


Figure 2. Schematic of Small Solid Propellant Motor.

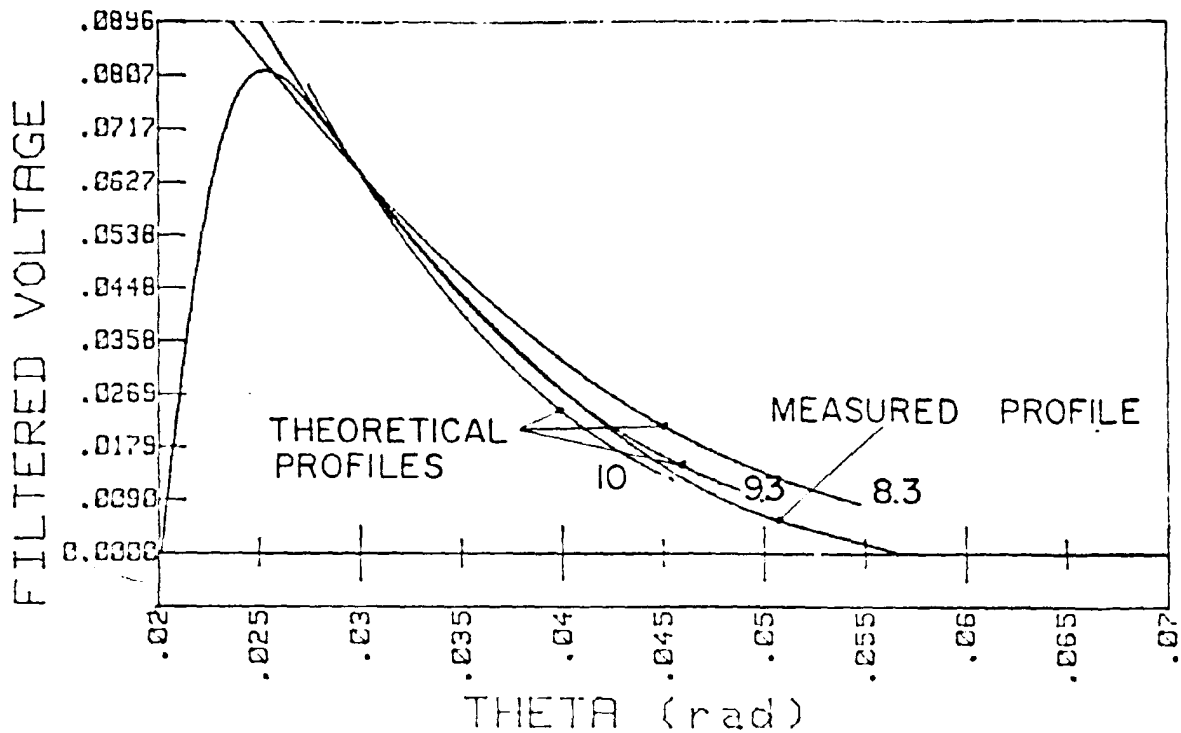


Figure 3. Measured and Theoretical Scattering Profiles for Particles with  $D_{32} = 10.2 \mu$

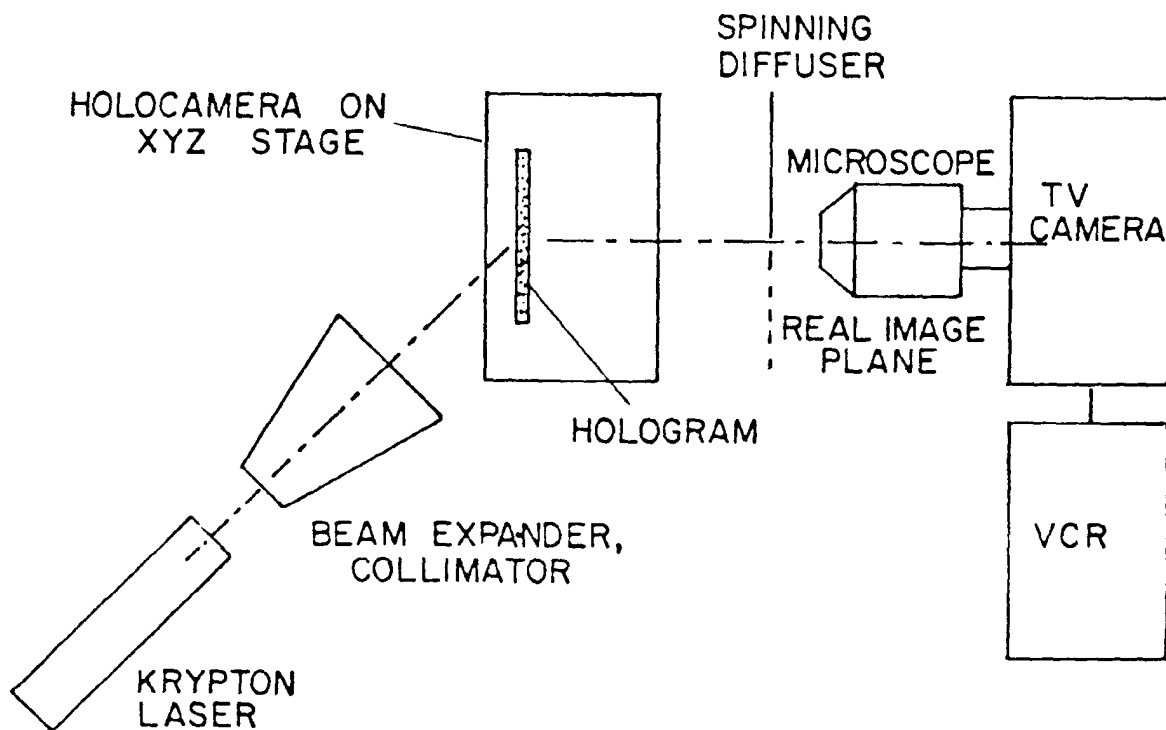
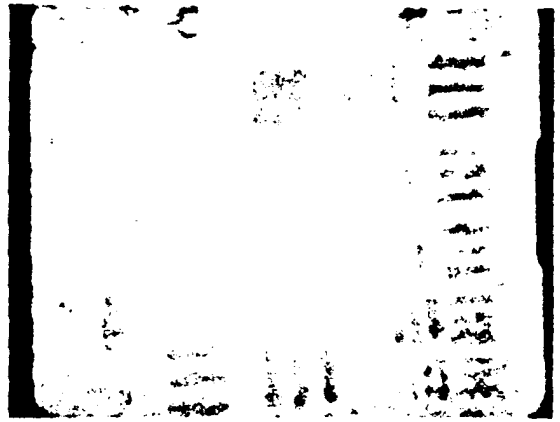
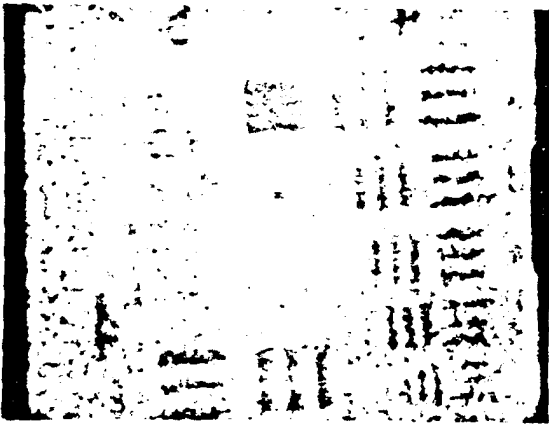
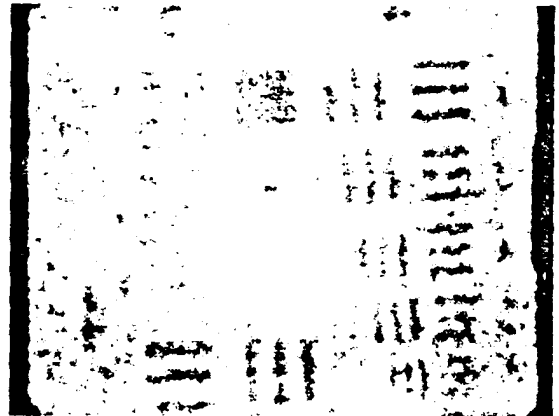
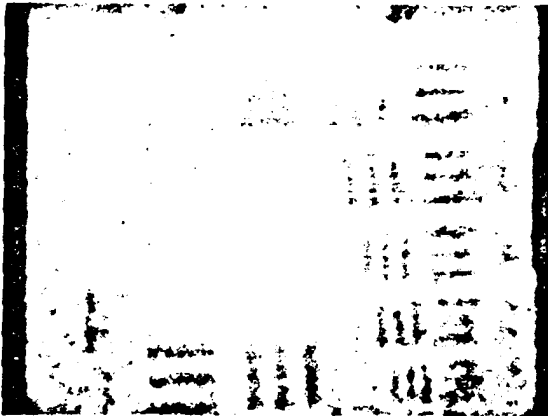


Figure 4. Image Recording Geometry.



(a) No filter, Speckle Index = 0.305

(b) With Geometric Filter, Speckle Index = 0.102



(c) With Sigma Filter, Speckle Index = 0.101

(d) With Statistical Filter, Speckle Index = 0.115

Figure 5. Comparison of speckle reduction methods in reconstructed holograms of the Air Force Resolution chart.

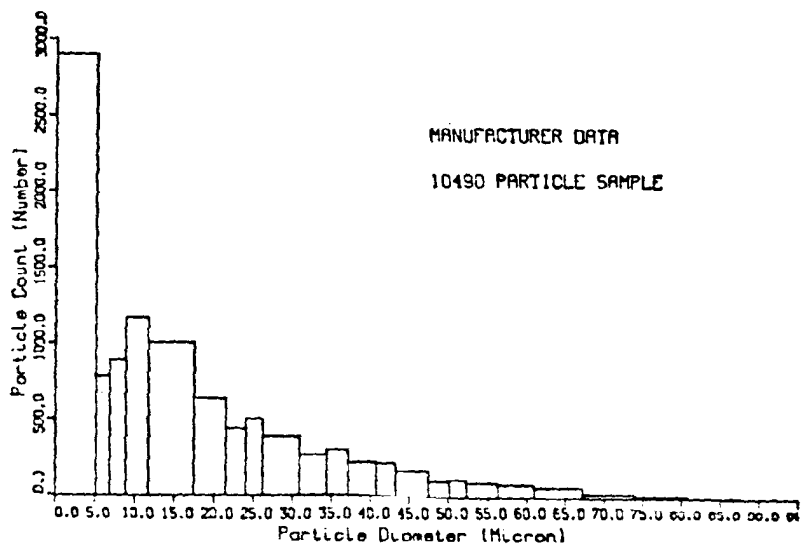


Figure 6. Histogram of calibration object.

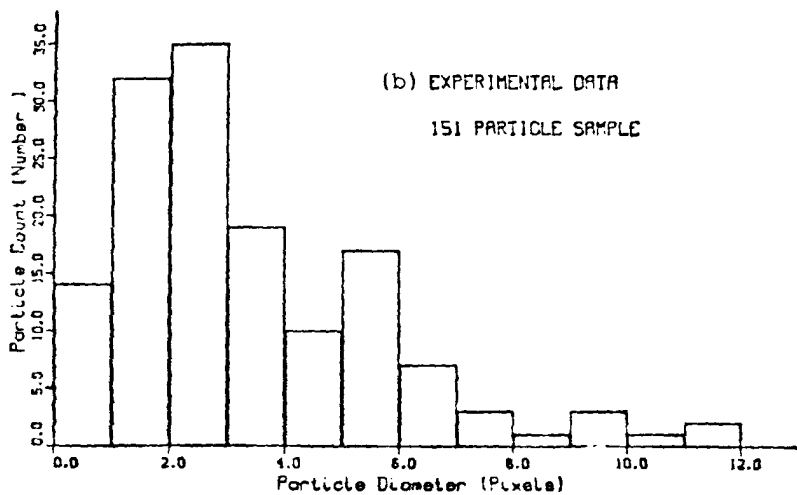
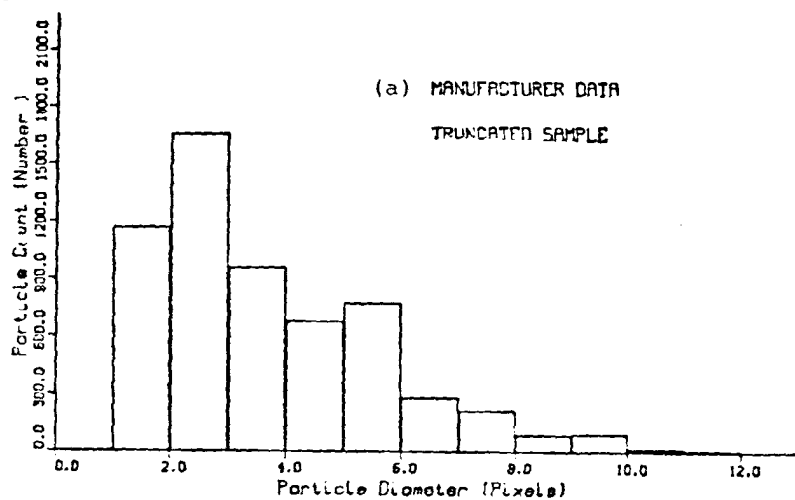


Figure 7. Histograms of calibration object, white light illumination.

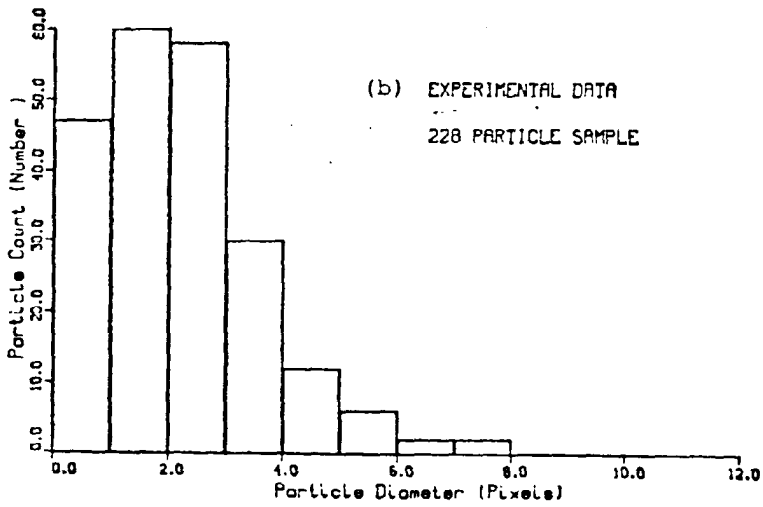
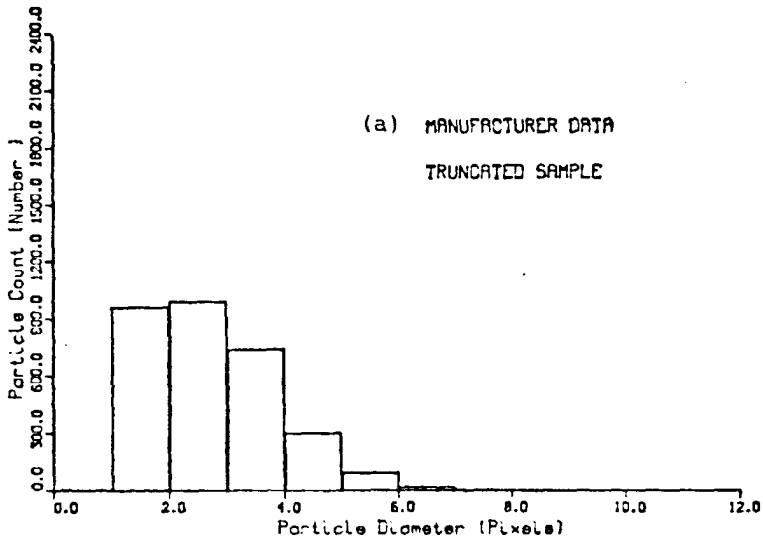


Figure 8. Histograms of calibration object, hologram reconstruction.